RESEARCH ARTICLE

Key Points:
- Complex refractive index data for 11 volcanic ash samples
- Explanation of methods used to find complex refractive indices
- Verification of methods through measurement of a calibration material

Correspondence to:
J. G. C. Ball,
ball.jgc@gmail.com

Measurements of the complex refractive index of volcanic ash at 450, 546.7, and 650 nm

J. G. C. Ball[1], B. E. Reed[1], R. G. Grainger[2], D. M. Peters[1], T. A. Mather[3], and D. M. Pyle[3]

[1] Atmospheric, Oceanic and Planetary Physics, University of Oxford, Oxford, UK, [2] COMET, Atmospheric, Oceanic and Planetary Physics, University of Oxford, Oxford, UK, [3] COMET, Earth Sciences, University of Oxford, Oxford, UK

Abstract The detection and quantification of volcanic ash is extremely important to the aviation industry, civil defense organizations, and those in peril from volcanic ashfall. To exploit the remote sensing techniques that are used to monitor a volcanic cloud and return information on its properties, the effective complex refractive index of the volcanic ash is required. This paper presents the complex refractive index determined in the laboratory at 450.0 nm, 546.7 nm, and 650.0 nm for volcanic ash samples from eruptions of Aso (Japan), Grímsvötn (Iceland), Chaitén (Chile), Etna (Italy), Eyjafjallajökull (Iceland), Tongariro (New Zealand), Askja (Iceland), Nisyros (Greece), Okmok (Alaska), Augustine (Alaska), and Spurr (Alaska). The Becke line method was used to measure the real part of the refractive index with an accuracy of 0.01. The values measured differed between eruptions and were in the range 1.51–1.63 at 450.0 nm, 1.50–1.61 at 546.7 nm, and 1.50–1.59 at 650.0 nm. A novel method is introduced to derive the imaginary part of the refractive index from the attenuation of light by ash. The method has a precision in the range 10^{-3}–10^{-4}. The values for the ash imaginary refractive index ranged 0.22–1.70×10^{-3} at 450.0 nm, 0.16–1.93×10^{-3} at 546.7 nm, and 0.15–2.08×10^{-3} at 650.0 nm. The accuracy of Becke and attenuation methods was assessed by measuring the complex refractive index of Hoya neutral density glass and found to have an accuracy of < 0.01 and $< 2 \times 10^{-5}$ for the real and imaginary parts of the refractive index, respectively.

1. Introduction

A volcanic eruption has the potential to cause a variety of severe and widespread threats to human well-being and the environment. Beyond the obvious calamitous effects to anyone in the immediate vicinity, eruptions are known to cause acute respiratory difficulties to people caught in an ashfall [*Horwell and Baxter*, 2006]. The injection of ash and sulfur dioxide into the atmosphere causes environmental damage and air quality issues [e.g., *Martin et al.*, 2009] and is a hazard and a huge financial burden to civil aviation stakeholders [*ICAO*, 2007]. It is therefore important that the dispersion of volcanic ash clouds is effectively monitored.

One way to acquire information on an eruption is through satellite observation. Images taken from space can cover large areas and so are able to provide a more complete view of an ash cloud than ground-based observations. However, a challenge of remote sensing is that certain properties of the target are often required (or need to be assumed) in order for accurate measurements to be made. For example, to acquire detailed information on a volcanic ash plume, a priori information on the size, shape, and optical properties of the constituent matter is needed or must be assumed [*Grainger et al.*, 2013].

Volcanic ash includes all pyroclasts of a diameter of less than 2 mm. The characteristics of the ash depend in part upon the eruptive process, but generally ash is composed of a mixture of vitric (glassy), crystalline, and lithic particles [*Schmid*, 1981]. Volcanic glass is formed by the quenching of magma during eruption. Crystalline material may include minerals that grew in the magma at depth before being expelled and smaller crystals that formed during the eruption of the magma. Rock or lithic fragments are present as a result of being broken off the walls of the magma conduit by the force of the eruptive flow [*Heiken and Wohletz*, 1985].

Observing a volcanic plume via satellite is possible as it perturbs the Earth's radiation field through absorption, scattering, and emission. How a particle scatters and absorbs light can be described by Mie theory for spherical particles, with additional techniques such as the T-Matrix approximation, the discrete dipole approximation, or ray tracing methods applicable to nonspherical particles [*Bohren and Huffman*, 1983]. With knowledge of the size distribution of the particles contained within a plume and their complex refractive index ($n + ik$) at a

Table 1. Previous Measurements of Refractive Indices of Volcanic Ash Samples and Materials

Sample	Refractive Index Component	Spectral Range (μm)	Reference
Volcanic ashes			
Mt. St Helens	k only	0.3–0.7	*Patterson* [1981]
El Chichón	k only	0.3–0.7	*Patterson et al.* [1983]
Mayon	k only	1–20	*Patterson* [1994]
Mt. Spurr	n and k	0.34, 0.36, 0.38	*Krotkov et al.* [1999]
Mt. Aso	n and k	1–20	*Grainger et al.* [2013]
Eyjafjallajökull	k only	0.3–2.5	*Rocha-Lima et al.* [2014]
Generic volcanic materials			
Basalt	n and k	0.4–50	*Pollack et al.* [1973]
		0.185–0.4	*Egan et al.* [1975]
Andesite	n and k	0.4–50	*Pollack et al.* [1973]
		0.185–0.4	*Egan et al.* [1975]
Pumice	n and k	0.2–40	*Volz* [1973]
Obsidian	n and k	0.21–40	*Pollack et al.* [1973]
Granite	n and k	5–40	*Toon et al.* [1977]

specific wavelength, these methods can be used to calculate the effect of ash on the shortwave radiation field [*Watson and Oppenheimer*, 2001]. In the infrared, instruments on board satellites can measure the attenuation of the Earth's field as the radiation passes from the Earth's surface, through an ash cloud, and up into space. The extinction coefficient calculated using Mie theory can then be used to deduce features such as the amount of ash present in the path [*Dubuisson et al.*, 2014]. Similarly, in the visible, measured levels of backscattered solar light from the ash can be used to deduce properties of the plume [*Nemuc et al.*, 2014].

Instruments that have been employed to monitor volcanic ash clouds include the Michaelson Interferometer for Passive Atmospheric Sounding [*Griessbach et al.*, 2014], the Advanced Along Track Scanning Radiometer [*Virtanen et al.*, 2014], and the Spinning Enhanced Visible and Infrared Imager (SEVIRI) [*Naeger and Christopher*, 2014]. *Francis et al.* [2012] describe the retrieval of ash properties from the 2010 Eyjafjallajökull eruption using data from the SEVIRI instrument, noting that their results were very sensitive to the choice of the assumed refractive indices. They obtained an observed plume mass in the range 0.308–0.825 Tg depending upon the assumed refractive index values. Without the availability of a refractive index specific to the ash, they settled on the very general values for the volcanic rock andesite [*Pollack et al.*, 1973].

Despite the obvious importance of knowing the complex refractive indices of volcanic ashes, existing measurements are limited. A list of the previously investigated ashes is provided in Table 1 along with the available data for various generic volcanic material. The data for the generic volcanic materials can be useful, but it only ever provides an approximation to real ash which is made up of a variety of different materials in many different forms. To be able to make maximum use of satellite imagery using modern precision instruments, the refractive indices of a range of ashes need to be determined.

One reason why it is difficult to assign values to the complex refractive index of volcanic ash is the fact that an ash sample from a single eruption will consist of a variety of different particles, often with varying optical properties. For example, fragments of volcanic glass can appear transparent, whereas the lithic particles can be almost completely opaque. *Ebert et al.* [2002] demonstrated that the overall complex refractive index of atmospheric aerosol samples, as determined by photometer measurements, could be matched within error bounds by retrieving the complex refractive indices of the individual particles and volume-averaging over the sample. Such an approach when applied to volcanic ash would mean that particles could be analyzed individually and their properties combined to produce an effective complex refractive index.

In this work, the complex refractive index for a set of volcanic ash samples is presented. Samples were chosen to capture a range of common SiO_2 contents of ash. A list of the ashes investigated along with some corresponding information is provided in Table 2. An application of the Becke line method was used to retrieve an overall value of the real part of the refractive index for 11 ash samples. A novel method, involving the

Table 2. Characterization of the Volcanic Ash Specimens[a]

Volcano	Eruption Date	SiO$_2$ Wt %	Number of Particles in Category			Average Particle Volume ($\times 10^6$ μm^3)	Average Aspect Ratio
			Clear	Intermediate	Opaque		
Aso	1993	52.55	18	6	6	0.31 $\pm$ 0.4	1.54 $\pm$ 0.41
Grímsvötn	5/2011	49.40	0	27	3	0.13 $\pm$ 0.1	1.71 $\pm$ 0.63
Chaitén[b]	2008	73.23	19	8	3	0.07 $\pm$ 0.1	1.58 $\pm$ 0.61
Etna	11/2002	47.14	10	6	14	0.31 $\pm$ 0.4	1.42 $\pm$ 0.41
Eyjafjallajökull	5/2010	58.03	7	14	9	1.2 $\pm$ 3.0	1.47 $\pm$ 0.30
Tongariro	11/2012	59.37	2	15	13	0.38 $\pm$ 0.7	1.40 $\pm$ 0.36
Askja[c]	1875 layer C	70.65	30	0	0	0.049 $\pm$ 0.03	1.74 $\pm$ 0.57
Nisyros[d]	?	69.67	23	4	3	0.018 $\pm$ 0.02	1.81 $\pm$ 0.73
Okmok	7/2008		5	18	8	0.1 $\pm$ 0.1	1.56 $\pm$ 0.53
Augustine[e]	1/2006		14	16	0	2.4 $\pm$ 2.0	1.38 $\pm$ 0.42
Spurr[f]	8/1992		12	11	7	2.0 $\pm$ 1.0	1.39 $\pm$ 0.33

[a]The SiO$_2$ weight percentage is from Prata et al. (in preparation). The particle categorization, average volume, and average aspect ratio come from the measurements described in section 2.2.2. Where available, references to how the samples were collected and processed are included.
[b]*Watt et al.* [2009].
[c]*Sparks et al.* [1981].
[d]*Longchamp et al.* [2011].
[e]*Larsen et al.* [2010].
[f]*Harbin et al.* [1995].

measurement of the imaginary part for individual particles within a sample, is presented and used to calculate an overall value of the imaginary part of the refractive index for the ash samples. This method is sensitive to particles typically larger than 10 μm in radius. The use of the refractive index values for smaller particles will be sensitive to any variation of the refractive indices with particle size.

2. Method

2.1. Real Part of the Refractive Index

The real part of the ash refractive index was measured using the Becke line method [*Becke*, 1896]. Briefly, this involves immersing a particle in a liquid of known refractive index. The sample is illuminated from below and viewed under a light microscope; the effects of refraction and total internal reflection cause a concentrated band of light (known as the Becke line) to form close to the fragment-liquid interface. Initially, the microscope is adjusted so an immersed particle is slightly above the focal point of the microscope's objective lens. As the particle is brought into focus the Becke line moves into the material with the higher refractive index. *Nesse* [2013] provides a detailed explanation of this phenomenon.

The ash samples under investigation were compared to a set of Cargille liquids of known refractive index. The set of 19 liquids ranged in refractive index from $n = 1.4600$ to $n = 1.6400$, separated by increments of 0.0100 (all with a standard error of ±0.0002). The laboratory was thermostatically regulated at 25°C, the temperature for which the liquids' Cauchy equations were accurate. About 3 mg of the ash was immersed in 50 mm^3 of liquid and shaken up to disperse the fragments uniformly. This ratio ensured that the fragments were well separated by the liquid, providing a clear view of the liquid-fragment boundaries. A couple of drops of the mixture were placed on a microscope slide and illuminated from below by halogen light filtered at 450.0 nm, 546.7 nm, or 650.0 nm. The filters had a bandpass of ±10 nm. The liquid refractive indices at the specified wavelengths were calculated using the Cauchy equation (coefficients were supplied by Cargille). The sample was observed with a 20X objective lens through the microscope eyepiece as well as via a CCD digital camera linked up to a computer monitor.

Different liquids were used until the Becke line was barely visible and the fragments appeared to blend with the surrounding mixture. If this was the case for all the particles, the ash would be assigned the same refractive index as that of the liquid. If all the Becke lines passed from the fragment into the liquid as the stage was

lowered for one liquid, but passed from the liquid into the fragment when placed in the incrementally higher liquid, the ash was assigned the refractive index halfway between the two liquids. It was not uncommon to see Becke lines passing in opposite directions, indicating the presence of particles of varying refractive index. If this were the case, a survey of 30 particles was undertaken, the number of particles going in each direction was counted, and an average value was calculated.

2.2. Imaginary Part of the Refractive Index

Previous studies have used diffuse reflectance techniques to find the imaginary component of the refractive index of a volcanic ash (as listed in Table 1). This approach identifies the value of k over a broad range of wavelengths but requires complex iterative procedures and forward modeling as well as knowledge of the size distribution of the ash and assumptions as to the shape of the contained particles. The technique presented here can be used to find k at discrete wavelengths in the visible spectrum. It is mathematically very simple and requires no knowledge of the size distribution of the ashes or of the shape of their particles.

In this method an ash sample was suspended in the Cargille liquid that most closely matched the real part of their refractive index at the illuminating wavelength. As the refractive index of the mounting liquid was approximately equal to the refractive index of the ash particles, light was assumed to pass straight through the particle, without changing direction due to refraction. In addition, the matching refractive indices meant that the reflectance at the particle-liquid boundary was negligible. It also follows that the reflectance at the slide-particle boundary was approximately equal to that at the slide-liquid boundary.

Essentially, the path of light which traveled through a particle was the same as the path of light which traveled past the particles and through the liquid, apart from the absorption of light that traveled through the particle. The spectral radiance of a ray passing through a particle, L_1, would have had an intensity which had been reduced according to

$$L_1 = L_0 e^{-\beta^{\mathrm{abs}} d}, \tag{1}$$

where L_0 was the illuminating radiance, β^{abs} was the volume absorption coefficient, and d was the path length of the light inside the particle. The volume absorption coefficient is related to the imaginary part of the refractive index k and the wavelength of light λ by

$$\beta^{\mathrm{abs}} = \frac{4\pi k}{\lambda}. \tag{2}$$

Combining equations (1) and (2) gives

$$k = \frac{\lambda}{4\pi d} \ln\left(\frac{L_0}{L_1}\right). \tag{3}$$

As it was observed that virtually no light was absorbed by the mounting medium, the spectral radiance entering the particle could be equated to the spectral radiance of the light passing through the slide unobstructed by the ash particles, as is illustrated in Figure 1.

2.2.1. Camera Calibration

The photographs taken from the CCD digital camera were stored as bitmap images, where each pixel had a red (R), green (G), and blue (B) coordinate, ranging from 0 to 255. The gamma correction applied to the images was set to 1 to avoid nonlinearity between input luminescence and output pixel coordinates. To convert pixel measurements to transmittance, neutral density filters of optical density (d) 0.1, 0.15, 0.2, 0.3, 0.6, 1, and 2 were used to provide known readings of transmittance and, hence, relative intensity. For each of the wavelengths of the filtered, illuminating light, a set of images was taken of the neutral density filters, as well as one of the unobstructed stage (100% transmittance) and one of the stage obstructed by a thick, opaque medium (0% transmittance). The brightness of the microscope lamp was set at each wavelength so that the maximum pixel value read just below 255 for photograph of the unobstructed stage, providing the widest possible range of values from which to calibrate the camera. The R (at 450 nm), G (at 546.7 nm), and B (at 650.0 nm) pixel values were shown to have a close linear correlation to the intensity of light with a small zero-point offset.
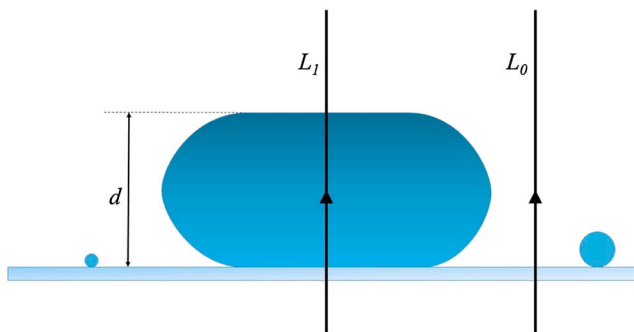
Figure 1. Diagram of two beams of light passing through the ash/liquid mixture. The beam labeled L_0 passes through unattenuated, whereas the beam labeled L_1 is partially absorbed while traveling through the ash particle with the length d indicating the path length of the light in the particle.

Relative intensity was related to the pixel value by

$$\frac{L_1}{L_0} = \frac{X_1 - c}{X_0 - c} \qquad (4)$$

where X_0 and X_1 were the R, G, or B pixel coordinates for the unobstructed and attenuated light, respectively, and c is the zero-point offset at the relevant wavelength. Substituting this into equation (3) led to an equation for k in terms of the relevant pixel value

$$k = \frac{\lambda}{4\pi d} \ln\left(\frac{X_0 - c}{X_1 - c}\right). \qquad (5)$$

2.2.2. Particle Measurements

Approximately 3 mg of ash was immersed in 60 mm^3 of the appropriate mounting liquid. The mixture was shaken vigorously to disperse the ash, and a few drops were placed on a microscope slide and covered with a cover slip. The sample was placed on the microscope stage and illuminated from below. An individual particle was selected, and the stage was positioned so that the particle was at the focal point of the microscope's 20X objective lens.

Photographs were taken of the ash particle in the matched medium. For each fragment investigated, the average color coordinate of a square of pixels at the center of the ash fragment was measured and assigned
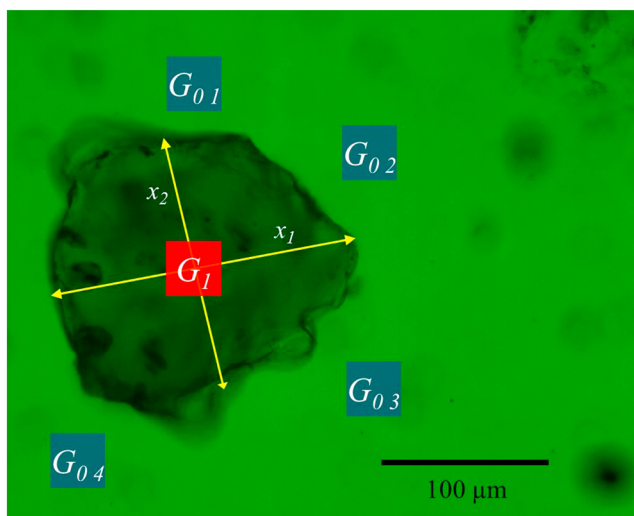
Figure 2. Photograph of a fragment of ash from the Spurr 8/1992 eruption with the 546.7 nm filter in place. The colored lines and boxes illustrate the parameters extracted from the image of an ash particle. In this case, the average G coordinate was extracted for a square of pixels at the center of the particle and for four unobstructed squares of pixels surrounding the particle. The perpendicular width and breadth measurements are also shown.

to the variable X_1. The average color coordinate for three or four unobstructed squares of pixels surrounding the fragment was also taken, then averaged and assigned to variable X_0. The length (x_1) and breadth (x_2) of the particle were also measured. An example of the extraction image is shown in Figure 2.

The relative vertical position of the base of the fragment was found by positioning the stage so that the microscope was focused on the upper surface of the glass slide. The position of the stage was read from the stage dial, which read to the nearest micrometer. The stage was then adjusted to focus on the upper surface at the center of the fragment, visible due to the tiny imperfections which existed on the fragment's surface. The new position was read from the dial, and its difference from the initial stage position was said to be the path length, d. The value of k was calculated from equation (5) and recorded for the particle. Lastly, the particle was assigned to a category of either *clear* (crystal or vitric), *opaque* (dark), or *intermediate*. This process was carried out for 30 particles in each sample, at each wavelength of light.

2.2.3. Generation of k From Individual Particle Measurements

To find a value for the imaginary part of the refractive index which was representative of the ash sample as a whole, an appropriate method of averaging the k values of the particles was required. Due to effects such as fragmentation of the erupted particles, there was no guarantee that chemical composition, and therefore k, was independent of particle size [*Zimanowski et al.*, 2003].

The ash samples were assumed to be an external mixture of individually homogeneous particles. Therefore, an effective imaginary part of the refractive index for the samples was calculated by taking a volume-weighted average of a sample of N particles:

$$k_{ash} = \frac{\sum_{i=1}^{N} V_i k_i}{\sum_{i=1}^{N} V_i} \tag{6}$$

where V_i values are the volumes of the individual particles. The exact morphology of the individual particles was not recorded. However, it could be considered reasonable to model an ash particle with width, length, and depth measurements as either an idealized cuboid or an idealized ellipsoid, and in both cases $V \propto x_1 x_2 d$. The fact that only the *relative* volume of the particles mattered meant that the product of the particle dimensions ($x_1 x_2 d$) could be taken to be a basis for the weights.

The uncertainties in the weighted sample mean k_{ash} were calculated from the weights of the individual particles and the standard deviations associated with their respective categories within the sample (clear, opaque, or intermediate).

2.3. Validation

To validate the method's ability to find the complex refractive index of volcanic ash, a control substance with a known complex refractive index was measured. A Hoya neutral density glass of class *ND-03* was used because of the following:

1. It had levels of attenuation similar to that of volcanic ash.
2. It was manufactured to be homogeneous throughout its structure.
3. The real part of the refractive index and the internal transmittance were precisely quoted over a wide range of wavelengths.

To roughly emulate the morphology and size distribution of volcanic ash, the glass was crushed, producing fragments varying in size and shape. The Becke line test was used to determine the real part of the refractive index for the control sample at 450.0 nm, 546.7 nm, and 650.0 nm. At each wavelength, the measured values matched the values quoted by the manufacturer to within the resolution set by the incrementation of the refractive index liquids ($\Delta n = 0.01$). The transmission method was used to retrieve the imaginary part of the refractive index. A comparison of the measured values to the manufacturer's quoted values is shown in Figure 3. At 650.0 nm the measurements show a close match to the value quoted by the manufacturer. However, at 450.0 nm and 546.7 nm the manufacturer's values were slightly below the measured values. As the differences ($< 2 \times 10^{-5}$) were less than the reported errors ($> 4 \times 10^{-5}$), usually by an order of magnitude, they were not investigated further.
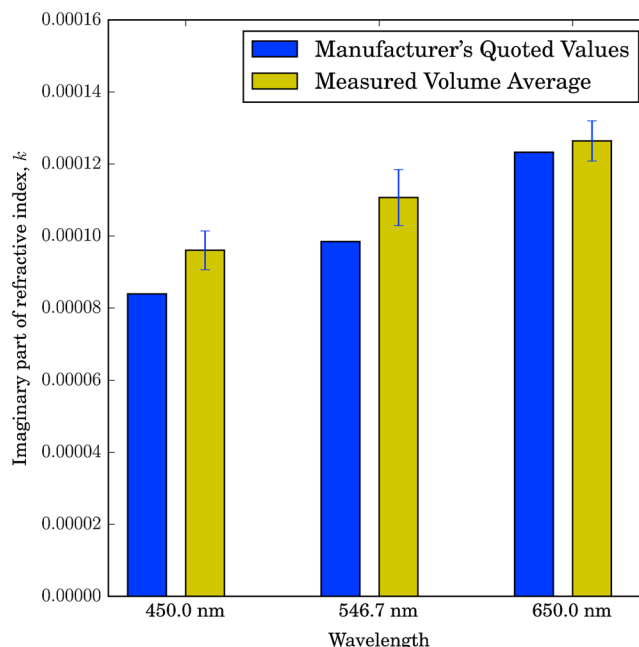
Figure 3. A comparison of the imaginary part of the refractive index of the Hoya neutral density glass and values retrieved using the transmission method. The errors are given by the standard deviation of the weighted sample mean, calculated from the individual particle weights and the spread in the measured k values.

3. Results

The real and imaginary parts of the refractive indices for 11 ash samples measured are listed in Tables 3 and 4, respectively. The real parts of the refractive index were measured to a precision of ± 0.01, determined by the resolution of mounting liquids. The ash with the smallest real part of the refractive index across all three wavelengths was Chaitén 2008 with values of 1.508 at 450.0 nm, 1.502 at 546.7 nm, and 1.499 at 650.0 nm. The ash with the largest real part of the refractive index across all three wavelengths was Grímsvötn 25/5/2011 with values of 1.629 at 450.0 nm, 1.608 at 546.7 nm, and 1.597 at 650.0 nm. Figure 4a shows that the expected

Table 3. The Real Part of the Index of Refraction for the Volcanic Ash Samples at 450.0 nm, 546.7 nm, and 650.0 nm, Measured Using the Becke Line Method[a]

	Real Part of the Refractive Index, n		
Ash Sample	450.0 nm	546.7 nm	650.0 nm
Aso 1993	1.577 ± 0.01	1.562 ± 0.01	1.553 ± 0.01
Grímsvötn 25/5/2011[b]	1.629 ± 0.01	1.608 ± 0.01	1.597 ± 0.01
Chaitén 2008	1.508 ± 0.01	1.502 ± 0.01	1.499 ± 0.01
Etna 01/11/2002[b]	1.605 ± 0.01	1.593 ± 0.01	1.582 ± 0.01
Eyjafjallajökull 15–16/5/2010[b]	1.561 ± 0.01	1.553 ± 0.01	1.554 ± 0.01
Tongariro 2012	1.537 ± 0.01	1.529 ± 0.01	1.527 ± 0.01
Askja	1.516 ± 0.01	1.510 ± 0.01	1.509 ± 0.01
Nisyros	1.520 ± 0.01	1.516 ± 0.01	1.515 ± 0.01
Okmok 7/2008[c]	1.594 ± 0.01	1.582 ± 0.01	1.579 ± 0.01
Augustine 13/1/2006[b]	1.535 ± 0.01	1.530 ± 0.01	1.529 ± 0.01
Spurr 8/1992[c]	1.570 ± 0.01	1.563 ± 0.01	1.555 ± 0.01

[a]The value of n is an average of ~ 30 sampled particles, and the uncertainties are from the resolution of the refractive index liquids used.
[b]Date formatted as day/month/year.
[c]Date formatted as month/year.

Table 4. The Imaginary Part of the Index of Refraction for the Volcanic Ash Samples at 450.0 nm, 546.7 nm, and 650.0 nm, Measured Using Our New Attenuation Method[a]

Ash Sample	Imaginary Part of the Refractive Index, k		
	450.0 nm	546.7 nm	650.0 nm
Aso 1993	0.00136 ± 0.00012	0.00124 ± 0.00018	0.00124 ± 0.00020
Grímsvötn 25/5/2011[b]	0.00155 ± 0.00027	0.00142 ± 0.00018	0.00129 ± 0.00017
Chaitén 2008	0.000314 ± 0.00012	0.000508 ± 0.00021	0.000471 ± 0.00018
Etna 01/11/2002[b]	0.00170 ± 0.00018	0.00193 ± 0.00021	0.00208 ± 0.00023
Eyjafjallajökull 15–16/5/2010[b]	0.000488 ± 0.00047	0.00108 ± 0.00058	0.000850 ± 0.00069
Tongariro 2012	0.000696 ± 0.00024	0.00106 ± 0.00029	0.00107 ± 0.00028
Askja	0.000221 ± 0.000083	0.000159 ± 0.000044	0.000147 ± 0.000039
Nisyros	0.000230 ± 0.000061	0.000325 ± 0.000094	0.000391 ± 0.00014
Okmok 7/2008[c]	0.00126 ± 0.00016	0.00145 ± 0.00023	0.00130 ± 0.00017
Augustine 13/1/2006[b]	0.000425 ± 0.00010	0.000549 ± 0.000097	0.000517 ± 0.00013
Spurr 8/1992[c]	0.000939 ± 0.00010	0.00105 ± 0.000083	0.00125 ± 0.00010

[a]The values of k are volume-weighted averages of ~30 sampled particles, and the uncertainties are from the standard deviations of the volume-weighted means.
[b]Date formatted as day/month/year.
[c]Date formatted as month/year.

dispersion relation at visible wavelengths was evident in all samples, with the real part of the refractive index decreasing with wavelength.

The imaginary part of the refractive index was measured for a sample of 30 particles within each of the 11 ash specimens. By volume averaging over the particles within each sample, an effective imaginary part of the refractive index was calculated. The overall values are displayed in Figure 4b.

Within a sample, the majority of the individual k measurements were clustered around a modal peak, with some samples showing secondary peaks at higher k values, demonstrating the different classes of particles
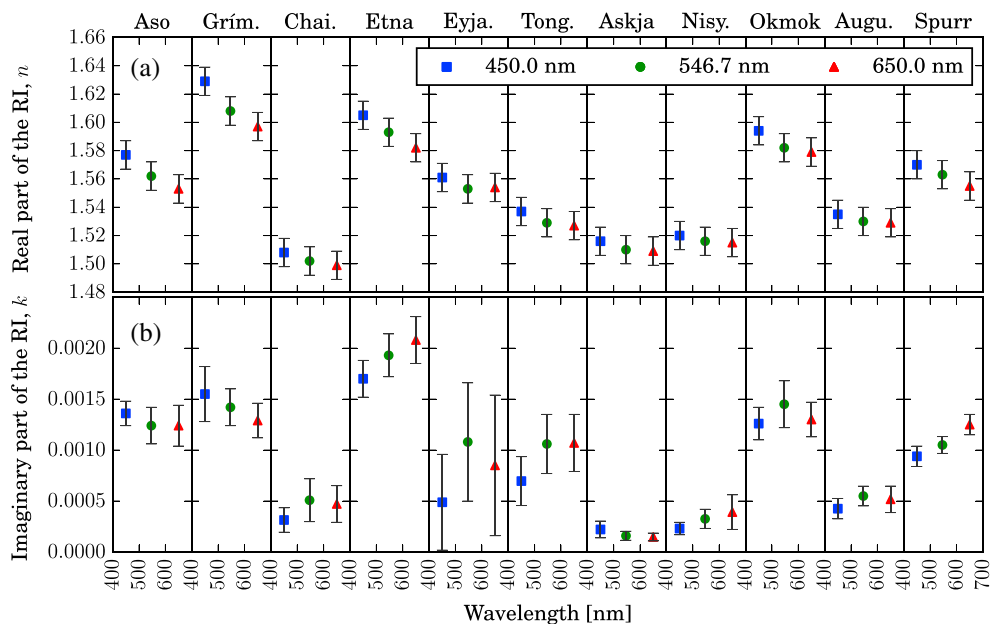
Figure 4. The (a) real and (b) imaginary parts of the refractive index for the ash samples at 450.0 nm, 546.7 nm, and 650.0 nm. The errors of the real parts are from the incrementation of the refractive index liquids. The errors in the weighted sample mean k_{ash} were calculated from the weights of the individual particles and the standard deviations associated with their respective categories within the sample.

present. Unsurprisingly, the particles with the lower values of k were generally classified as clear and the intermediate and opaque particles were more highly absorbing.

Within the given errors the results for k of the Eyjafjallajökull 15–16/5/2010 ash matched those for Eyjafjallajökull ash investigated by *Rocha-Lima et al.* [2014] at 546.7 nm and 650.0 nm. The value of k at 450.0 nm was below that given by *Rocha-Lima et al.* [2014]. Nonetheless, the proximity of these results for differently retrieved samples is encouraging. The values of k for the ashes in *Patterson* [1981] and *Patterson et al.* [1983], at the wavelengths under investigation in this paper, were in the range 0.0006–0.004. This fits reasonably well with the values of k found by the transmission method.

Across all three wavelengths the Etna 01/11/2002 ash was measured to be the most highly absorbing with values of the imaginary part of the refractive index of 0.00170 at 450.0 nm, 0.00193 at 546.7 nm, and 0.00208 at 650.0 nm. The sample was formed predominantly of dark finely crystalline particles. Furthermore, even the clear glass particles appear more absorbing compared to the clear glass particles within the other samples.

Across all three wavelengths the Askja ash was measured to have the smallest values of the imaginary part of the refractive index with values of 0.000221 at 450.0 nm, 0.000159 at 546.7 nm, and 0.000147 at 650.0 nm. All particles measured in this sample appeared glassy and were categorized as clear.

There was a large variation in the errors associated with each of the different samples. The error in k for the Eyjafjallajökull 15–16/5/2010 ash was especially large; indeed, it was comparable to the retrieved value. The particles within this sample were particularly difficult to classify. Not only were the clear, intermediate, and opaque groups not easily spotted, but the particles themselves were not homogeneous. The particles were often dark in parts but clear in others, while some contained fused fragments or bubbles encased in glass. The Spurr 8/1992 ash, on the other hand, exhibited the smallest relative error. The particles within this sample could be classified with ease, and the particles were quite tightly distributed about the modal values of each group.

4. Discussion and Conclusions

The Becke line method is a standard procedure and returned good results. The resolution for some ashes could have been increased had liquids of a finer refractive index incrementation been used. The averaging procedure was not as rigorous as the volume averaging technique used in the transmission method, but the variation in n observed within a sample was generally small, and recording the volume as well as the refractive index of each particle would not have yielded notably different results. The expected dispersion relation of n decreasing with wavelength was visible in all samples. This provided reassurance and suggested that the errors attached to these results, taken from the incrementation of the refractive index liquids, were too large. The Becke line test was validated by the match between the manufacturer's quoted values and the measured values of n for the Hoya ND-03 glass at all three wavelengths.

The transmission method returned values of the imaginary part of the refractive index with varying degrees of precision. The values were based on a survey of 30 ash particles per ash specimen. A larger sample would have provided more precise results, but for most ashes the sample size of 30 gave results with error bars that were small relative to the value and allowed time for a range of ashes to be studied. An independent study with a survey of a different set of 30 particles from within the same samples would demonstrate reproducibility and provide increased confidence in the results.

While the current measurements provide a useful reference in the visible, measurements of ash refractive indices over a wider spectral range (0.35–15 μm) are required to fully exploit remote measurements.

The overall k values calculated by volume averaging the values of the constituent particles required the assumption that the ashes were an external mixture of particles, each of a uniform consistency. However, in the Chaitén, Eyjafjallajökull, and Nisyros ash samples there existed fragments that were either fused from a mixture of different materials or contained bubbles of volcanic gas causing a breakdown in the above assumption. The inhomogeneities within the particles would mean that the particles have a broad range of k values rather than falling into the three distinct distributions of clear, opaque, and intermediate. In turn, this would have led to a larger standard deviation in the measurements and a larger standard error associated with the overall value of k. There has been some debate as to whether volume-averaging the constituent materials of a particle can be used to find an effective refractive index of atmospheric aerosol particles which are internally

mixed [*Bohren and Huffman*, 1983; *Gillespie et al.*, 1978; *Lindberg et al.*, 1993]. It has been suggested that the Bruggeman and Maxwell Garnett mixing rules may map the constituent parts of an individual particle to its overall effect more accurately [*Chýlek et al.*, 1988]. However, the large errors associated with the samples for which the external mixing assumption was not entirely valid incorporate the necessary caution with which our results for the Chaitén, Eyjafjallajökull, and Nisyros ash samples should be viewed. It should also be noted that the results for *k* for the Chaitén, Eyjafjallajökull, and Nisyros ash samples are likely to be overestimates, as extinction which was taken to be due to absorption would have been actually, at least in part, caused by scattering due to inhomogeneities within the particles themselves.

A limitation of the particle absorption method was that it was unable to test the particles with a size parameter lower than about 120 due to the sensitivity of the camera (at visible wavelengths this corresponds to particles with a radius of less than about 10 μm). These particles, although individually small, constitute a large combined volume within each sample. Furthermore, there is evidence that smaller aerosol particles are relatively more absorbing [*Lindberg and Gillespie*, 1977] so that the current method may bias *k* to a value smaller than that for the distribution as a whole and they are expected to experience longer atmospheric lifetimes than larger particles, hence contributing more to the optical properties of the older, dispersed plumes that are often of interest especially in terms of aviation hazards. In future work the samples could be filtered so that only the finest particles remain. They could then be suspended in a liquid of a matched refractive index, and the extinction could be measured. Providing they are small enough, the Rayleigh approximation would mean that extinction would be entirely due to absorption, and the imaginary part of the refractive index could be retrieved and compared to that of the larger particles measured in this paper.

The disparity between the quoted and measured values of *k* for the Hoya ND-03 glass at 450.0 nm and 546.7 nm was small but concerning. The fact that the measured and quoted values aligned at 650.0 nm signifies that the disparity was caused by an unaccounted-for refractive effect which is therefore more significant at shorter wavelengths.

The chemical composition of a volcanic ash plays a key role in governing its optical properties. The silica content has been observed to have a close relationship to both real and imaginary parts of the refractive index. Further research into the relationship of the complex refractive index of volcanic ash with its composition is to be encouraged. This would aid rapid estimation of refractive indices for real-time remote sensing during eruptive crises.

References

Becke, F. J. K. (1896), Beziehungen zwischen Dynamometamorphose und Moldkularcolumen, *Neues Jahrb. Mineral.*, *2*, 182–183.

Bohren, C. F., and D. R. Huffman (1983), *Absorption and Scattering of Light by Small Particles*, John Wiley, New York.

Chýlek, P., V. Srivastava, R. G. Pinnick, and R. T. Wang (1988), Scattering of electromagnetic waves by composite spherical particles: Experiment and effective medium approximations, *Appl. Opt.*, *27*(12), 2396–2404, doi:10.1364/AO.27.002396.

Dubuisson, P., H. Herbin, F. Minvielle, M. Compiègne, F. Thieuleux, F. Parol, and J. Pelon (2014), Remote sensing of volcanic ash plumes from thermal infrared: A case study analysis from SEVIRI, MODIS and IASI instruments, *Atmos. Meas. Tech.*, *7*(2), 359–371, doi:10.5194/amt-7-359-2014.

Ebert, M., S. Weinbruch, A. Rausch, G. Gorzawski, P. Hoffmann, H. Wex, and G. Helas (2002), Complex refractive index of aerosols during LACE 98 as derived from the analysis of individual particles, *J. Geophys. Res.*, *107*(D21), 8121, doi:10.1029/2000JD000195.

Egan, W., T. Hilgeman, and K. Pang (1975), Ultraviolet complex refractive-index of Martian dust: Laboratory measurements of terrestrial analogs, *Icarus*, *25*(2), 344–355, doi:10.1016/0019-1035(75)90029-9.

Francis, P. N., M. C. Cooke, and R. W. Saunders (2012), Retrieval of physical properties of volcanic ash using Meteosat: A case study from the 2010 Eyjafjallajökull eruption, *J. Geophys. Res.*, *117*, D00U09, doi:10.1029/2011JD016788.

Gillespie, J. B., S. G. Jennings, and J. D. Lindberg (1978), Use of an average complex refractive index in atmospheric propagation calculations, *Appl. Opt.*, *17*(7), 989–991, doi:10.1364/AO.17.000989.

Grainger, R. G., D. M. Peters, G. E. Thomas, A. J. A. Smith, R. Siddans, E. Carboni, and A. Dudhia (2013), Measuring volcanic plume and ash properties from space, in *Remote Sensing of Volcanoes and Volcanic Processes: Integrating Observation and Modelling*, edited by D. M. Pyle, T. A. Mather, and J. Biggs, *Geol. Soc. London Spec. Publ.*, *380*, 293–320, doi:10.1144/SP380.7.

Griessbach, S., L. Hoffmann, R. Spang, and M. Riese (2014), Volcanic ash detection with infrared limb sounding: MIPAS observations and radiative transfer simulations, *Atmos. Meas. Tech.*, *7*(5), 1487–1507, doi:10.5194/amt-7-1487-2014.

Harbin, M., S. Swanson, C. Nye, and T. Miller (1995), Preliminary petrology and chemistry of proximal eruptive products; 1992 eruptions of Crater Peak, Mount Spurr Volcano, Alaska, in *The 1992 Eruptions of Crater Peak Vent, Mount Spurr Volcano, Alaska, U.S. Geol. Surv. Bull.*, vol. 2139, edited by T. Keith, pp. 139–148, U.S. Geol. Surv., Reston, Va.

Heiken, G., and K. H. Wohletz (1985), *Volcanic Ash*, Univ. of California Press, Berkeley, Calif.

Horwell, C. J., and P. J. Baxter (2006), The respiratory health hazards of volcanic ash: A review for volcanic risk mitigation, *Bull. Volcanol.*, *69*, 1–24.

ICAO (2007), *Manual on Volcanic Ash, Radioactive Material and Toxic Chemical Clouds*, ICAO Doc 9691, Int. Civil Aviat. Organ., Montreal Quebec, Can.

Krotkov, N. A., D. E. Flittner, A. J. Krueger, A. Kostinski, C. Riley, W. Rose, and O. Torres (1999), Effect of particle non-sphericity on satellite monitoring of drifting volcanic ash clouds, *J. Quant. Spectrosc. Radiat. Transfer*, *63*(2–6), 613–630, doi:10.1016/S0022-4073(99)00041-2.

Larsen, J. F., C. J. Nye, M. L. Coombs, M. Tilman, P. Izbekov, and C. Cameron (2010), Petrology and geochemistry of the 2006 eruption of Augustine Volcano, in *The 2006 Eruption of Augustine Volcano, Alaska, U.S. Geol. Surv. Prof. Pap.*, vol. 1769, edited by J. A. Power, M. L. Coombs, and J. T. Freymueller, chap. 15, pp. 335–382, U.S. Geol. Surv., Reston, Va.

Lindberg, J. D., and J. B. Gillespie (1977), Relationship between particle size and imaginary refractive index in atmospheric dust, *Appl. Opt.*, *16*(10), 2628–2630, doi:10.1364/AO.16.002628.

Lindberg, J. D., R. E. Douglass, and D. M. Garvey (1993), Carbon and the optical properties of atmospheric dust, *Appl. Opt.*, *32*(30), 6077–6081, doi:10.1364/AO.32.006077.

Longchamp, C., C. Bonadonna, O. Bachmann, and A. Skopelitis (2011), Characterization of tephra deposits with limited exposure: The example of the two largest explosive eruptions at Nisyros volcano (Greece), *Bull. Volcanol.*, *73*(9), 1337–1352, doi:10.1007/s00445-011-0469-9.

Martin, R., S. Watt, D. Pyle, T. Mather, N. Matthews, B. Georg, J. Day, T. Fairhead, M. Witt, and B. Quayle (2009), Environmental effects of ashfall in Argentina from the 2008 Chaitén volcanic eruption, *J. Volcanol. Geotherm. Res.*, *184*, 462–472, doi:10.1016/j.jvolgeores.2009.04.010.

Naeger, A. R., and S. A. Christopher (2014), The identification and tracking of volcanic ash using the Meteosat Second Generation (MSG) Spinning Enhanced Visible and Infrared Imager (SEVIRI), *Atmos. Meas. Tech.*, *7*(2), 581–597, doi:10.5194/amt-7-581-2014.

Nemuc, A., I. S. Stachlewska, J. Vasilescu, A. Gorska, D. Nicolae, and C. Talianu (2014), Optical properties of long-range transported volcanic ash over Romania and Poland during Eyjafjallajökull eruption in 2010, *Acta Geophys.*, *62*(2), 350–366, doi:10.2478/s11600-013-0180-7.

Nesse, W. D. (2013), *Introduction to Optical Mineralogy*, Int. 4th ed., Oxford Univ. Press, New York.

Patterson, E. M. (1981), Measurements of the imaginary part of the refractive index between 300 and 700 nanometers for Mount St. Helens ash, *Science*, *211*(4484), 836–838, doi:10.1126/science.211.4484.836.

Patterson, E. M. (1994), Optical absorption coefficients of soil-aerosol particles and volcanic ash between 1 and 16 μm, paper presented at the Second Conference on Atmospheric Radiation, pp. 177–180, Arlington, Va., 29–31 Oct. 1975.

Patterson, E. M., C. O. Pollard, and I. Galindo (1983), Optical properties of the ashes from El Chichon volcano, *Geophys. Res. Lett.*, *10*(4), 317–320, doi:10.1029/GL010i004p00317.

Pollack, J. B., O. B. Toon, and B. N. Khare (1973), Optical properties of some terrestrial rocks and glasses, *Icarus*, *19*(3), 372–389, doi:10.1016/0019-1035(73)90115-2.

Rocha-Lima, A., J. V. Martins, L. A. Remer, N. A. Krotkov, M. H. Tabacniks, Y. Ben-Ami, and P. Artaxo (2014), Optical, microphysical and compositional properties of the Eyjafjallajökull volcanic ash, *Atmos. Chem. Phys. Discuss.*, *14*(9), 13,271–13,300, doi:10.5194/acpd-14-13271-2014.

Schmid, R. (1981), Descriptive nomenclature and classification of pyroclastic deposits and fragments: Recommendations of the IUGS subcommission on the systematics of igneous rocks, *Geology*, *9*(1), 41–43, doi:10.1130/0091-7613(1981)9<41:DNACOP>2.0.CO;2.

Sparks, R. S. J., L. Wilson, and H. Sigurdsson (1981), The pyroclastic deposits of the 1875 eruption of Askja, Iceland, *Philos. Trans. R. Soc. A*, *299*(1447), 241–273, doi:10.1098/rsta.1981.0023.

Toon, O. B., J. B. Pollack, and C. Sagan (1977), Physical properties of the particles composing the Martian dust storm of 1971–1972, *Icarus*, *30*(4), 663–696, doi:10.1016/0019-1035(77)90088-4.

Virtanen, T. H., P. Kolmonen, E. Rodríguez, L. Sogacheva, A.-M. Sundström, and G. de Leeuw (2014), Ash plume top height estimation using AATSR, *Atmos. Meas. Tech.*, *7*(8), 2437–2456, doi:10.5194/amt-7-2437-2014.

Volz, F. E. (1973), Infrared optical constants of ammonium sulfate, Sahara dust, volcanic pumice, and flyash, *Appl. Opt.*, *12*(3), 564–568, doi:10.1364/AO.12.000564.

Watson, I. M., and C. Oppenheimer (2001), Photometric observations of Mt. Etna's different aerosol plumes, *Atmos. Environ.*, *35*(21), 3561–3572, doi:10.1016/S1352-2310(01)00075-9.

Watt, S., D. Pyle, T. Mather, R. Martin, and N. Matthews (2009), Fallout and distribution of volcanic ash over Argentina following the May 2008 explosive eruption of Chaitén, Chile, *J. Geophys. Res.*, *114*, B04207, doi:10.1029/2008JB006219.

Zimanowski, B., K. Wohletz, P. Dellino, and R. Büttner (2003), The volcanic ash problem, *J. Volcanol. Geotherm. Res.h*, *122*(1), 1–5.